

UNIVERSITY OF WATERLOO  
Physics and Astronomy

IMPLEMENTATION OF THE  
PHASE SPACE TOMOGRAPHY  
ALGORITHM

TRIUMF  
Vancouver, BC

Prepared by  
Dan Sehayek  
ID #20628857  
dsehayek@uwaterloo.ca  
2B Mathematical Physics  
April 27, 2018

# Table of Contents

<b>Abstract</b> . . . . .	<b>v</b>
<b>1.0 Acknowledgements</b> . . . . .	<b>1</b>
<b>2.0 Introduction</b> . . . . .	<b>2</b>
<b>3.0 Analysis</b> . . . . .	<b>4</b>
3.1 2D Phase Space Tomography Routine . . . . .	4
3.2 Simulated Data . . . . .	5
3.3 View Screen Data . . . . .	8
3.4 Web Application . . . . .	15
<b>4.0 Conclusions</b> . . . . .	<b>19</b>
<b>5.0 Recommendations</b> . . . . .	<b>20</b>
<b>A Phase Space</b> . . . . .	<b>21</b>
<b>B Lattice Elements</b> . . . . .	<b>24</b>
<b>References</b> . . . . .	<b>26</b>

# List of Figures

1	A visual representation of the method in which tomography is applied. The left figure represents an unknown phase space distribution at the location of interest. The middle figure represents this distribution after the beam passes through a ramping element (RE). The right figure represents the measured beam profile after the beam passes through the selected profile monitor (PM). This would be repeated for multiple settings after which both the profiles and corresponding transfer matrices would be provided to MENT. . . . .	4
2	A simulated elliptical distribution and its corresponding MENT reconstruction. Five increments of $15^\circ$ were used for the rotation matrices. Colours represent spatial densities and are computed using a Gaussian kernel. . . . .	5
3	This contour plot shows the variation of the phase space reconstruction error with respect to $N$ and $\theta$ for a tilted ellipse distribution. . . . .	6
4	A simulated S shaped distribution and its corresponding MENT reconstruction. Eighteen increments of $5^\circ$ were used for the rotation matrices. . . . .	7
5	Variation of the phase space reconstruction error with respect to $N$ and $\theta$ for an S shaped distribution. . . . .	7
6	View screen data from EGUN:CAMVS1 after cropping the image and applying a sobel filter. Additional for loops were used to remove smaller contours resulting from the filter. . . . .	9
7	Reconstruction of horizontal phase space using profiles obtained from ELBT:VS2 with EGUN:SOL1 as the ramping element. .	11
8	Reconstruction of vertical phase space using profiles obtained from ELBT:VS2 with EGUN:SOL1 as the ramping element. .	11
9	4 of the 14 original $x$ profiles obtained from the view screen data and the corresponding fitted profiles provided by MENT. . . .	12
10	4 of the 14 original $y$ profiles obtained from the view screen data and the corresponding fitted profiles provided by MENT. . . .	12
11	The integrals of each of the $x$ profiles obtained from the view screen data calculated using a Simpson integrator. . . . .	13
12	The integrals of each of the $y$ profiles obtained from the view screen data calculated using a Simpson integrator. . . . .	13

13	The RMS <sup>2</sup> values of each of the $x$ profiles obtained from the view screen data. The plot takes the form of a parabola as expected. . . . .	14
14	The RMS <sup>2</sup> values of each of the $y$ profiles obtained from the view screen data. The plot takes the form of a parabola as expected. . . . .	14
15	First half of the scan interface for the tomography application. <i>Generated Datafiles</i> shows the name of the raw datafiles that have currently been uploaded and their corresponding settings. <i>Options</i> allows the user to select a profile monitor and start the scan process. If the user begins to notice issues such as beam loss, the scan can be aborted. Once the scan is complete, the user will be allowed to immediately run tomography. Finally, <i>More Options</i> allows the user to view the default XML specifying the ramping elements and settings for the current configuration as well as upload their own XML file if they would like to use a different ramping element or list of settings. . . . .	17
16	Second half of the scan interface for the tomography application. Similar to the webpage responsible for showing the MENT output, the user can view the post processed $x$ and $y$ profiles as well as the integral and RMS plots. The integral and RMS plots can be used to determine if the scan is not running correctly and needs to be aborted. . . . .	18
17	Visual representation of the Frenet Serret coordinate system. The red point represents the reference point at which $s = 0$ and the black line represents the design orbit. . . . .	21
18	Graph of the phase space ellipse corresponding to Equation 2.	22
19	Multipoles corresponding to the first three orders. Top left is a dipole, top right is a quadrupole and bottom is a sextupole. Red and blue correspond to North and South respectively. Black lines indicate magnetic field lines. . . . .	25

## List of Tables

1	RMS and $\varepsilon$ values for the $x - x'$ phase space. . . . .	10
2	RMS and $\varepsilon$ values for the $y - y'$ phase space. . . . .	10

# Abstract

The concept of measuring beams in phase space has proven to be a very effective tool in accelerator physics for understanding beam dynamics and improving beamlines. While this task can be accomplished using emittance scanners, they are slow and expensive and cannot be used in certain beamline locations due to their large size. This report focuses on the implementation of a phase space tomography algorithm that aims to reconstruct phase space distributions using an extended version of Maximum Entropy Tomography (MENT). The algorithm is first tested on simulated data generated using multivariate distributions and is then tested on real profiles obtained from view screen data. In the case of view screen data, MENT attempts to reconstruct at the exit of EGUN:ACC using ELBT:VS2 as the view screen and EGUN:SOL1 as the ramping element. Reconstructions from the simulated data show promising accuracy and present a method of determining optimal settings for specified configurations. Emittance values from reconstructions from the view screen data agree with expected values from TRANSOPTR by a percent difference of 0.037% and emphasize the possibility of using view screens and image processing to measure profiles.

## 1.0 Acknowledgements

I would like to thank my supervisors Carla Barquest, Thomas Planche and Suresh Saminathan and the rest of the Accelerator Division for the incredible learning experiences and support that they provided me with throughout my 8 month coop at TRIUMF. During my time at TRIUMF, I was given the opportunity to work on numerous projects focused on the development and implementation of algorithms such as multipole tuning and phase space tomography, each of which required me to learn and apply several skills ranging from optimization and scientific computing to web development and image processing. I was additionally given the amazing opportunity to write a paper for the IPAC 2018 conference for the multipole tuning algorithm. The countless opportunities that I was given to develop as an undergraduate physicist and as a researcher have made this experience unforgettable and invaluable and I owe it all to my team and the people that made this possible.

In regards to the phase space tomography algorithm, I would like to give an additional thanks to Paul Jung, Samantha Marcano and David Tattan for their previous work on the implementation of phase space tomography and the development of its web application. Their work was a crucial part of this project and the progress in this report would not have been achieved if it were not for their previous contributions.

## 2.0 Introduction

The concept of tomography or reconstructing an unknown object from an arbitrary number of projections is one that is constantly used in many areas of science and engineering including particle physics and medical imaging. In recognition of this, researchers are constantly optimizing algorithms responsible for tomography with the goal of improving accuracy and efficiency. In 1979, Gerald Minerbo developed a tomography algorithm with the goal of reconstructing 2D distributions from 1D profiles. This algorithm was named Maximum Entropy Tomography (MENT) [1] and proved to have superior performance relative to many other algorithms that had been developed before then such as the Multiplicative Algebraic Reconstruction Technique (MART). Since then, many efforts have been placed to optimize the algorithm further and many have considered the application of such an algorithm to a common problem in accelerator physics: reconstructing the phase space distribution of a beam at any given longitudinal coordinate along a beamline. As a result, an extended version of MENT has been developed with the specific goal of reconstructing phase space distributions using ramping elements to apply linear transformations to the beam of interest. In addition to the 1D profiles, the transfer matrix corresponding to each setting/profile is also provided in order to allow for reconstruction at the specified location.

In the context of accelerator physics, phase space is a mathematical tool that provides a simple and effective method to studying and predicting the motion and position of a given beam as it travels along a beamline. In general, we will be interested in knowing the  $x$  vs  $x'$  and  $y$  vs  $y'$  distributions where  $'$  denotes differentiation with respect to the longitudinal coordinate  $s$ . A more detailed description of the motivation and mathematics behind phase space

is given in Appendix A. Ultimately, the ability to accurately and efficiently obtain the phase space distribution at any desired point along a beamline will allow accelerator physicists to deeply improve their understanding of beam dynamics and enable them to further optimize the structure and specifications of beamlines. While emittance scanners are effective at completing such a task, they are slow and expensive and are simply impractical to install at every location where operators may want to reconstruct the beam's phase space. Thus it is necessary to establish an alternative method to completing such reconstructions. This report focuses on assessing the effectiveness of MENT in regards to reconstructing phase space using both clean generated data and real data. The real data used in this report was obtained using the ELBT:VS2 view screen and will allow us to assess the possibility of using image processing techniques to obtain profiles as opposed to the traditional profile monitors.

## 3.0 Analysis

### 3.1 2D Phase Space Tomography Routine

This section focuses on describing the extended version of MENT for 2D phase space tomography. A complete description of this routine can be found in [2]. As previously mentioned, the goal of MENT is to reconstruct an unknown 2D distribution from multiple 1D projections. In the context of phase space, these 1D profiles are measured using a profile monitor that is selected based on the desired reconstruction location. In order to obtain several profiles, a ramping element that the beam travels through after the reconstruction location and before the profile monitor is set to several different currents/voltages. Since ramping elements such as quadrupoles correspond to linear transformations, this allows the beam to experience multiple rotations and thus allows us to obtain a set of distinct 1D profiles. The transfer matrices corresponding to each setting that this extended version of MENT additionally requires are obtained using a beam envelope code known as TRANSOPTR [3]. A visual summary of this description is shown in Figure 1.

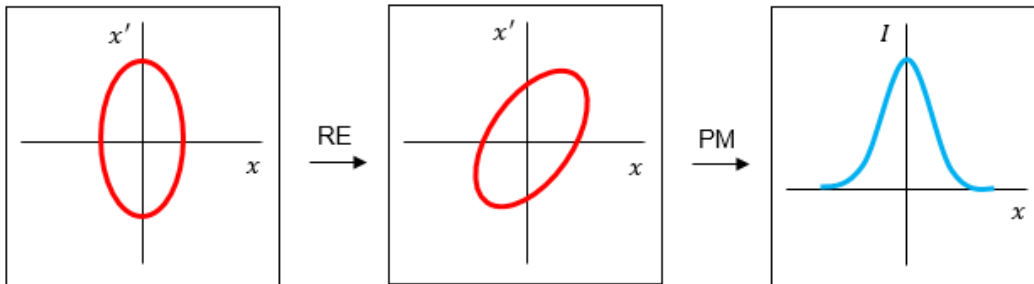


Figure 1: A visual representation of the method in which tomography is applied. The left figure represents an unknown phase space distribution at the location of interest. The middle figure represents this distribution after the beam passes through a ramping element (RE). The right figure represents the measured beam profile after the beam passes through the selected profile monitor (PM). This would be repeated for multiple settings after which both the profiles and corresponding transfer matrices would be provided to MENT.

### 3.2 Simulated Data

Before testing the MENT algorithm on real data, the algorithm was first tested on simulated data in order to allow for comparisons between the reconstructed distributions and the actual distributions. The first case that was considered was a simple tilted ellipse. This distribution was generated using a multivariate method from NumPy with  $\vec{\mu} = \vec{0}$  as the center and  $\sigma = \begin{pmatrix} 3 & 1 \\ 1 & 1 \end{pmatrix}$  as the covariance matrix and is shown in Figure 2.

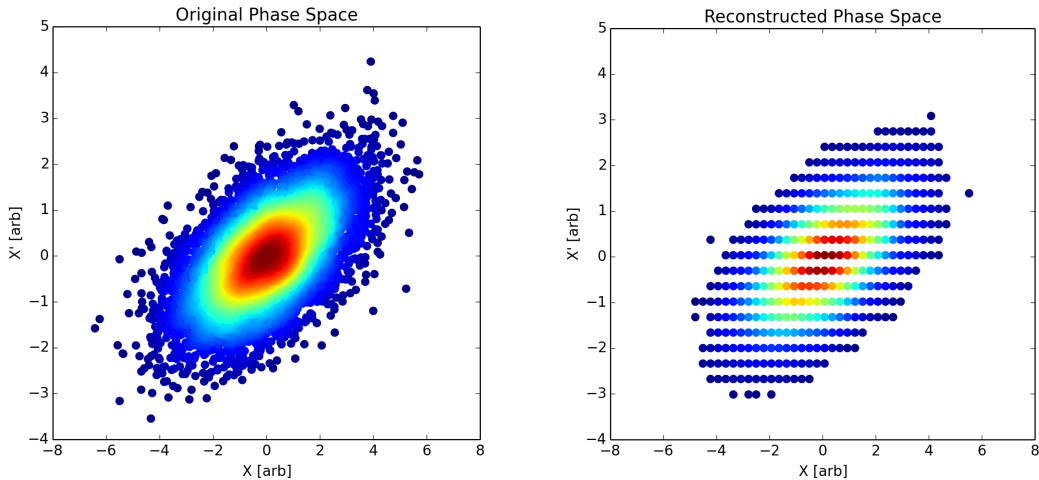


Figure 2: A simulated elliptical distribution and its corresponding MENT reconstruction. Five increments of  $15^\circ$  were used for the rotation matrices. Colours represent spatial densities and are computed using a Gaussian kernel.

In general, the transfer matrices will vary depending on the type of ramping element selected. However, since the ultimate goal of applying these transformations is to apply rotations, simple rotation matrices were used. In order to determine the optimal set of rotations, two parameters were optimized: the number of angular increments  $N$  and the value of each angular increment  $\theta$ . The starting angle is set to  $0^\circ$ . For the example shown in Figure 2, all possible combinations of  $N \in [4, 19]$  in increments of 1 and  $\theta \in [5^\circ, 45^\circ]$  increments of  $5^\circ$  were considered and the values providing the optimal reconstruction were

used. In this case,  $N = 5$  and  $\theta = 15^\circ$  provided the minimum reconstruction error. Note that the error  $\epsilon$  is computed by applying a linear interpolation of the original and reconstructed data onto a consistent 2D grid and summing the squared differences.  $Q_{\max}$  was not used as an accuracy metric as it measures the error based on the fitted profiles and can provide low values for poor reconstructions. An optimization landscape showing the variation of the reconstruction error with respect to  $N$  and  $\theta$  is shown in Figure 3.

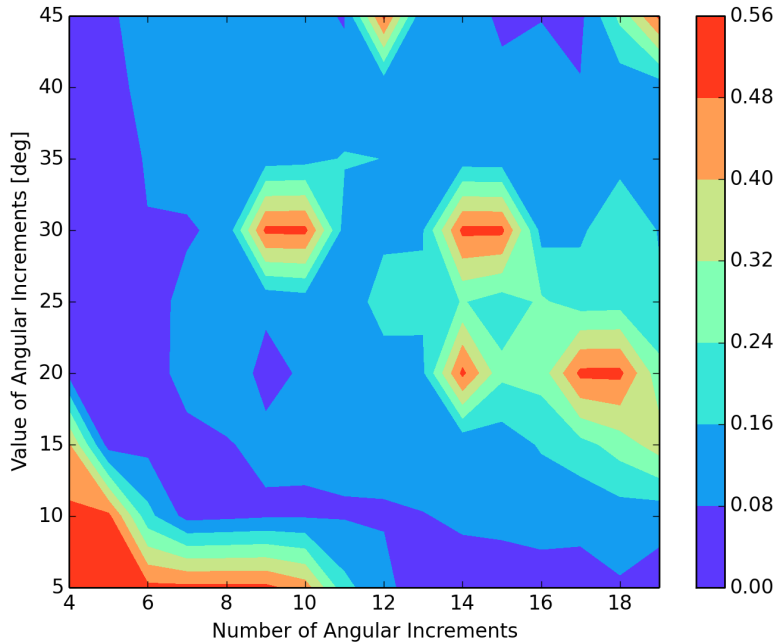


Figure 3: This contour plot shows the variation of the phase space reconstruction error with respect to  $N$  and  $\theta$  for a tilted ellipse distribution.

Following the elliptical distribution, the MENT algorithm was tested on several other distributions created by first generating an upright ellipse and then applying a horizontal shift characterized by a polynomial function. Figure 4 shows one of these distributions. This specific distribution was generated by first applying a multivariate method with  $\vec{\mu} = \vec{0}$  and  $\sigma = \begin{pmatrix} 0 & 1 \\ 1 & 0 \end{pmatrix}$  and then shifting each point horizontally by the value corresponding to a cubic function ( $x = Ax^3$ ). The corresponding optimization landscape is shown in Figure 5.

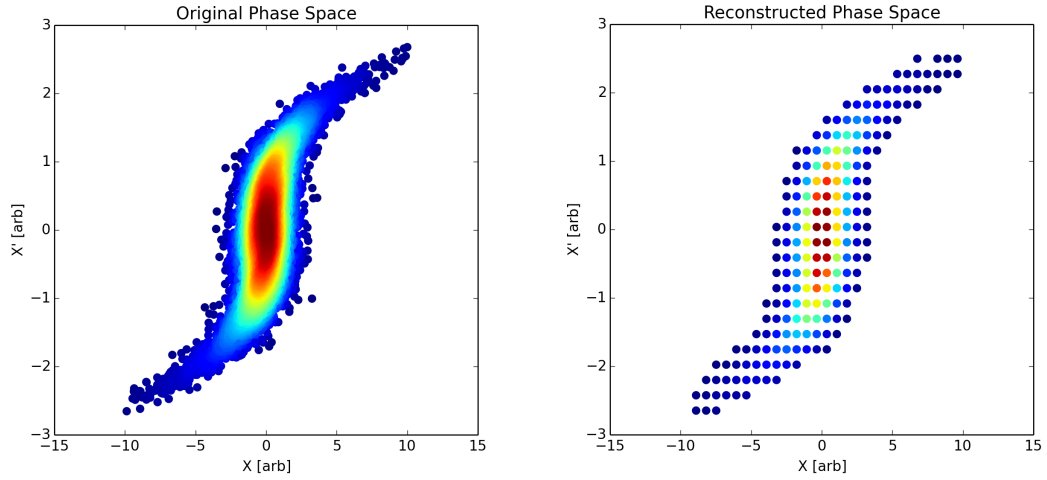


Figure 4: A simulated S shaped distribution and its corresponding MENT reconstruction. Eighteen increments of  $5^\circ$  were used for the rotation matrices.

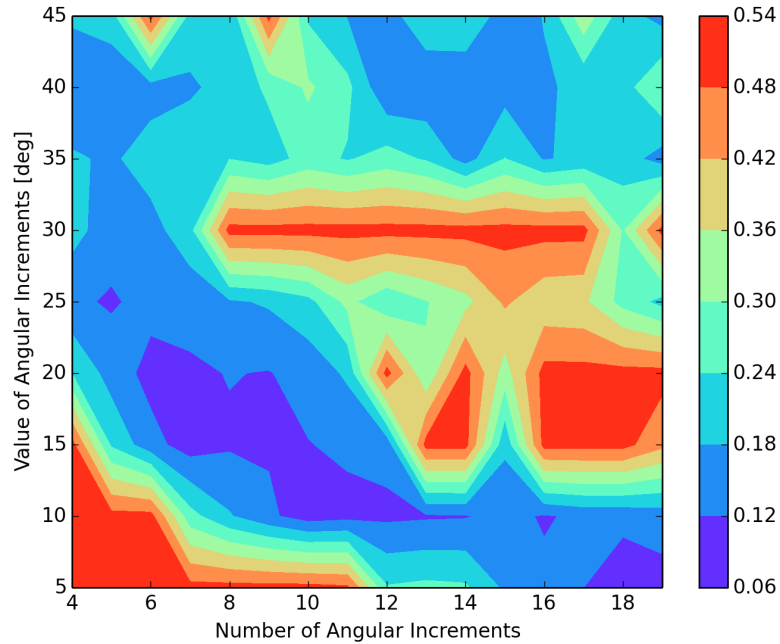


Figure 5: Variation of the phase space reconstruction error with respect to  $N$  and  $\theta$  for an S shaped distribution.

In general, the optimal settings will depend on the type of distribution being reconstructed and the type of ramping element being used. The results from the reconstructions shown above as well as the success of additional reconstructions not shown in this report emphasize that the phase space tomography algorithm can perform accurate reconstructions of phase space distributions if an optimal set of transformations is applied. Furthermore, this method of selecting optimal settings/rotations can be used to help determine if a current set of selected settings is the reason for obtaining poor reconstructions for any tomography attempts involving real data.

### 3.3 View Screen Data

The original method of acquiring 1D profiles was to select a profile monitor that measures the beam after it passes through the reconstruction location and the ramping element. Multiple profiles can then be obtained simply by applying multiple settings and measuring the profiles for each of these settings. Such a method was applied by D. Tattan [4] to a 18.4 kV Li7 beam using IMS:RPM18 as the profile monitor and IMS:Q18 as the ramping element and had considerable success.

This section focuses on using view screen data to obtain the 1D profiles instead of typical profile monitors. In the case of view screen data, the greyscale value of each pixel can be used as a relative measure for the number of particles at that location. The corresponding 1D profiles can be obtained by summing the greyscale values of each pixel along each column or row depending on whether an  $x$  or  $y$  profile is desired. Before summing these values, it is necessary to apply a filter in order to distinguish relevant pixels from background pixels. Many effective filters were found from skimage [5], a Python module

for image processing. Figure 6 shows an example of processed view screen data from EGUN:CAMVS1 after applying a sobel filter and additional filtering of resulting minor contours.

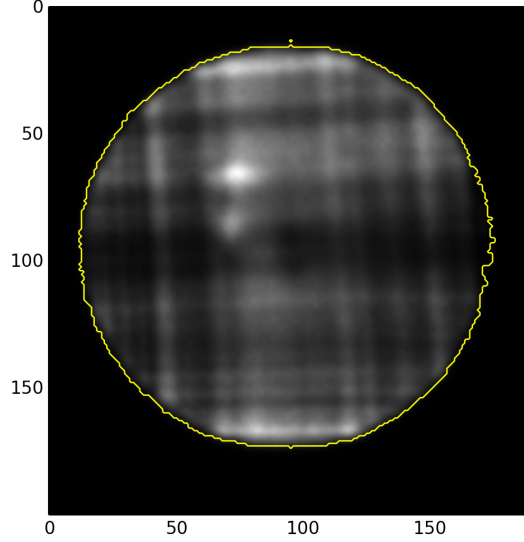


Figure 6: View screen data from EGUN:CAMVS1 after cropping the image and applying a sobel filter. Additional for loops were used to remove smaller contours resulting from the filter.

This process for obtaining profiles was applied to tomography in the egun-einj beampath using the exit of EGUN:ACC as the reconstruction location, EGUN:SOL1 as the ramping element and ELBT:VS2 as the view screen. 14 profiles were produced while varying the current on the solenoid from 2.12 A to 2.58 A. In addition to the cropping and filtering, each of the view screen images were rotated to allow the coupling terms of the solenoid transfer matrices to be ignored and thus allow for 2D transfer matrices. These angles were calculated using Equation 1. For this particular case,  $\int Bdl = (7.29 \cdot 140 \text{ G} \cdot \frac{\text{cm}}{\text{A}}) \cdot I$  where  $I$  is the current applied to the solenoid and  $B\rho = 2.1 \cdot 10^{-3} \text{ T} \cdot \text{m}$ .

$$\theta = \frac{\int Bdl}{B\rho} \quad (1)$$

The horizontal and vertical phase space reconstructions are shown in Figures 7 and 8 respectively. Additionally, 4 of the 14 original and fitted  $x$  and  $y$  profiles are shown in Figures 9 and 10 and the RMS<sup>2</sup> and integral plots of these profiles are shown in Figures 11, 12, 13 and 14. In order to assess the accuracy of the reconstructions, the expected RMS and emittance values were determined by fitting the beam’s initial conditions to the calculated beam envelope using TRANSOPTR. Tables 1 and 2 show these values along with the values obtained from MENT for the  $x - x'$  and  $y - y'$  phase space distributions. Ultimately, the percent differences in the emittance values for both reconstructions were 0.037%. While no immediate conclusions can be made to the success of the reconstructions without the use of an emittance scanner, the results are promising and emphasize that further efforts should be placed into the development and implementation of this routine. The parabolic relationships shown in Figures 13 and 14 as well as the ability of MENT to fit the 1D profiles additionally emphasize that the new image processing routine designed for measuring profiles from view screen data was successful and may prove to be another useful tool for completing tomographic reconstructions.

Table 1: RMS and  $\epsilon$  values for the  $x - x'$  phase space.

	TRANSOPTR Value	MENT Value
$2\sqrt{\langle x^2 \rangle}$	0.167 cm	0.130 cm
$2\sqrt{\langle x'^2 \rangle}$	0.0272 rad	0.0250 rad
$r_{12}$	0.971	0.947
$\epsilon$	10.9 $\mu\text{m}$	10.5 $\mu\text{m}$

Table 2: RMS and  $\epsilon$  values for the  $y - y'$  phase space.

	TRANSOPTR Value	MENT Value
$2\sqrt{\langle y^2 \rangle}$	0.167 cm	0.142 cm
$2\sqrt{\langle y'^2 \rangle}$	0.0272 rad	0.0240 rad
$r_{12}$	0.971	0.951
$\epsilon$	10.9 $\mu\text{m}$	10.5 $\mu\text{m}$

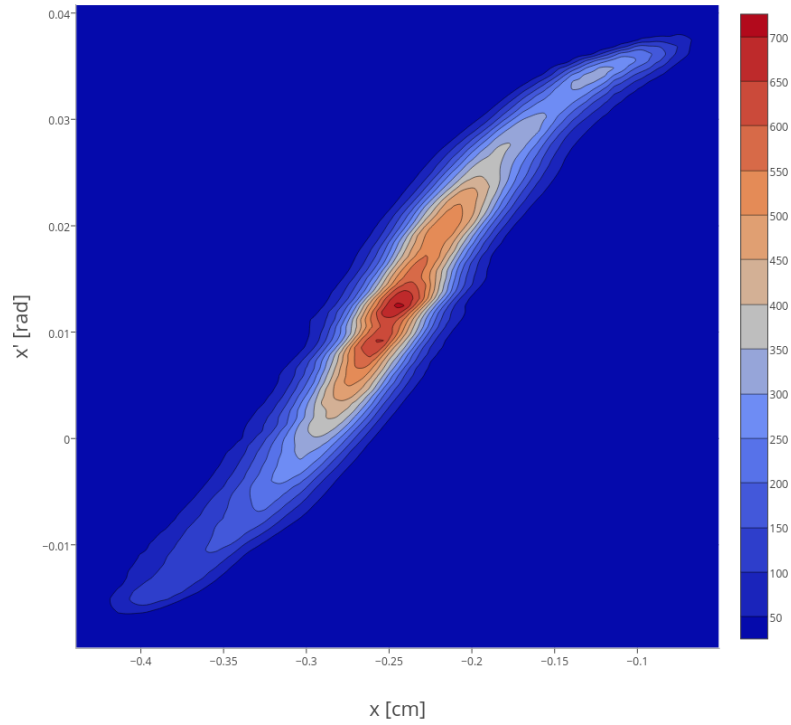


Figure 7: Reconstruction of horizontal phase space using profiles obtained from ELBT:VS2 with EGUN:SOL1 as the ramping element.

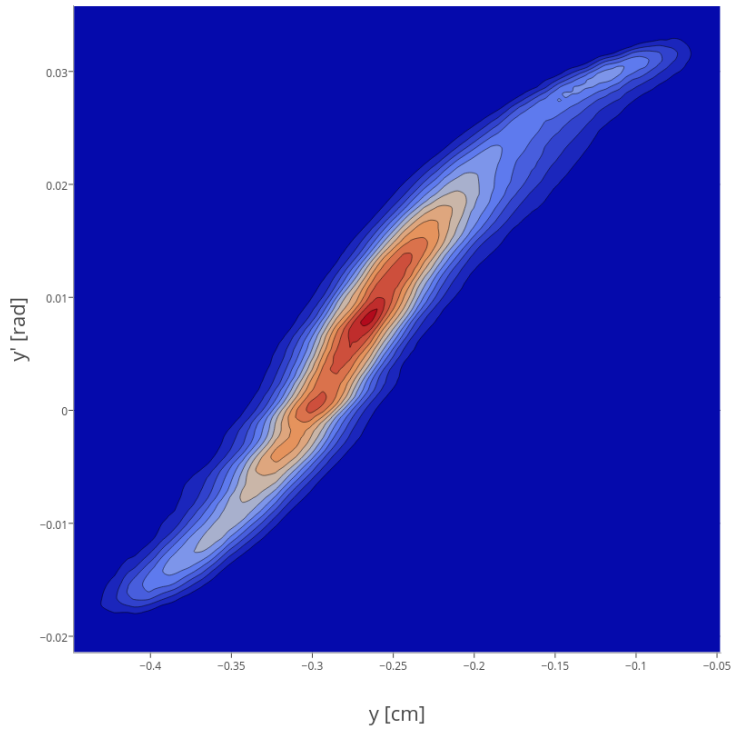


Figure 8: Reconstruction of vertical phase space using profiles obtained from ELBT:VS2 with EGUN:SOL1 as the ramping element.

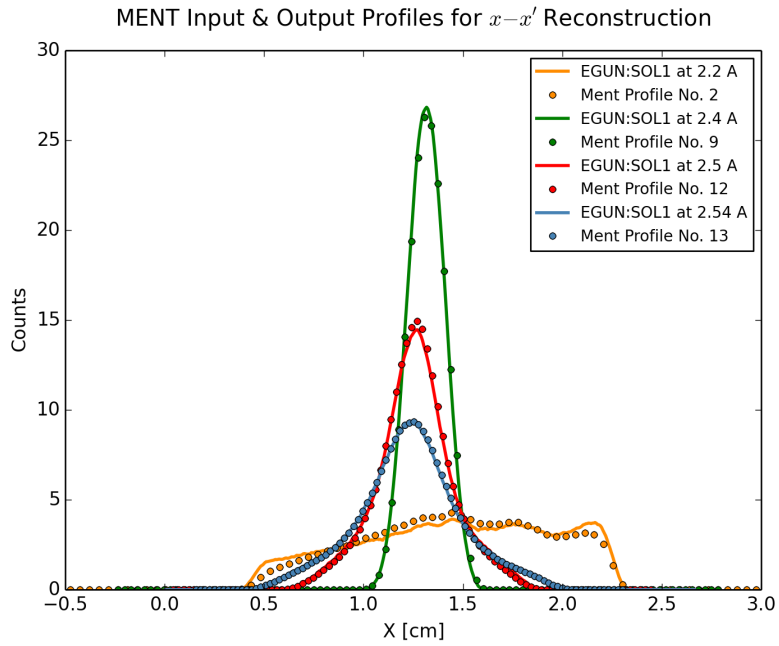


Figure 9: 4 of the 14 original  $x$  profiles obtained from the view screen data and the corresponding fitted profiles provided by MENT.

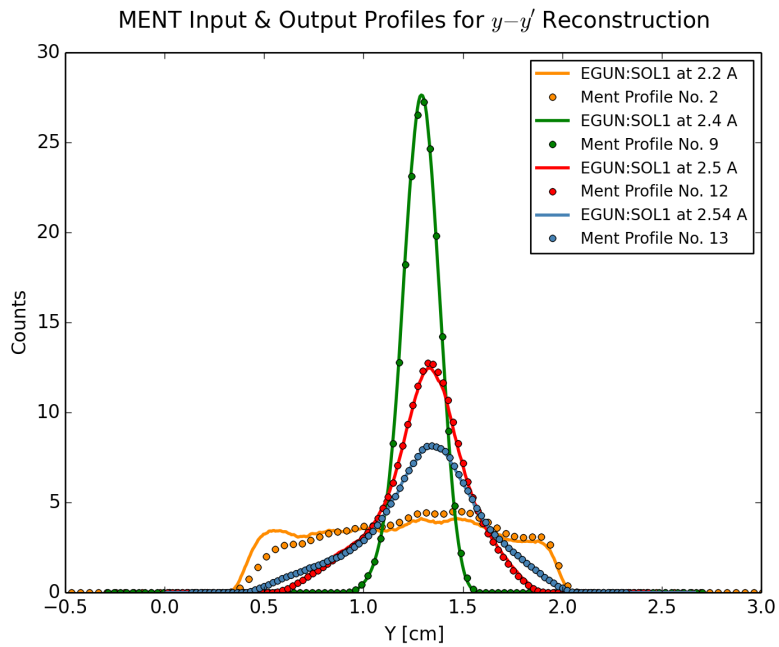


Figure 10: 4 of the 14 original  $y$  profiles obtained from the view screen data and the corresponding fitted profiles provided by MENT.

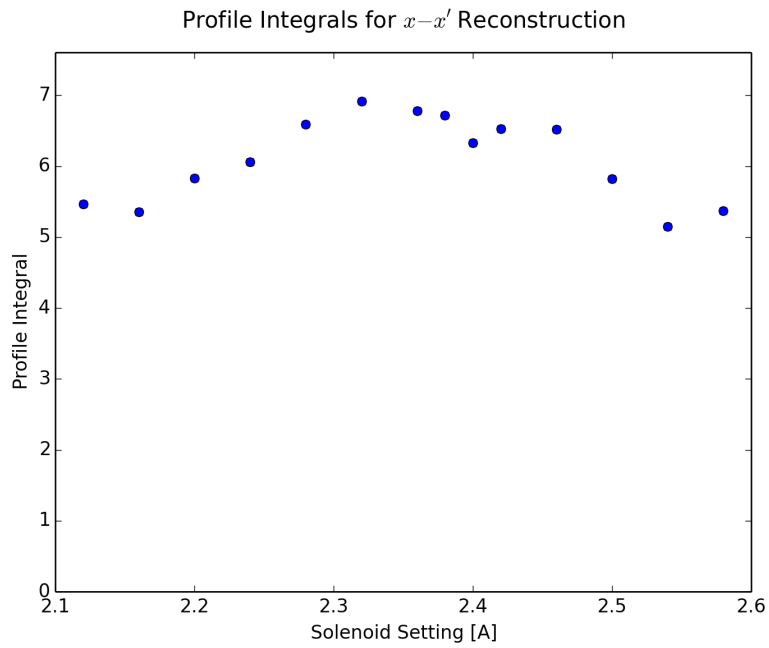


Figure 11: The integrals of each of the  $x$  profiles obtained from the view screen data calculated using a Simpson integrator.

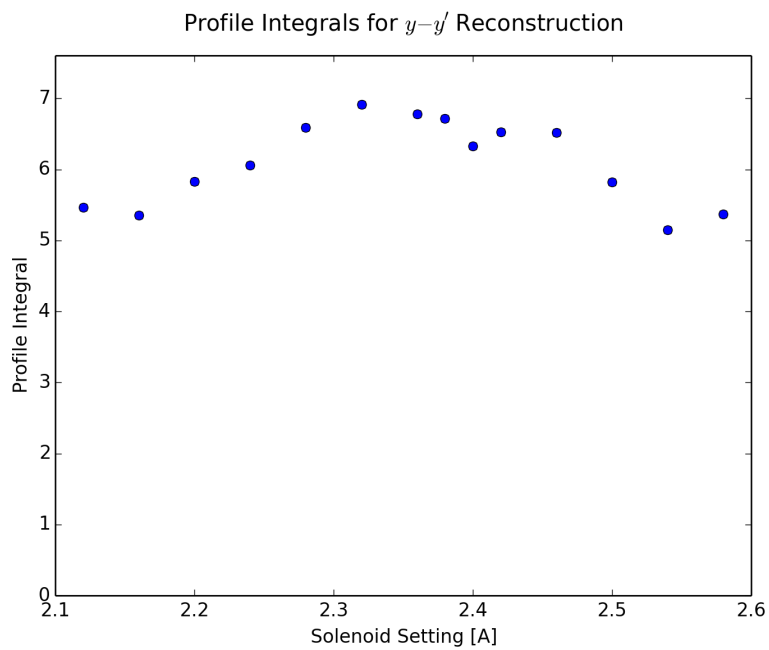


Figure 12: The integrals of each of the  $y$  profiles obtained from the view screen data calculated using a Simpson integrator.

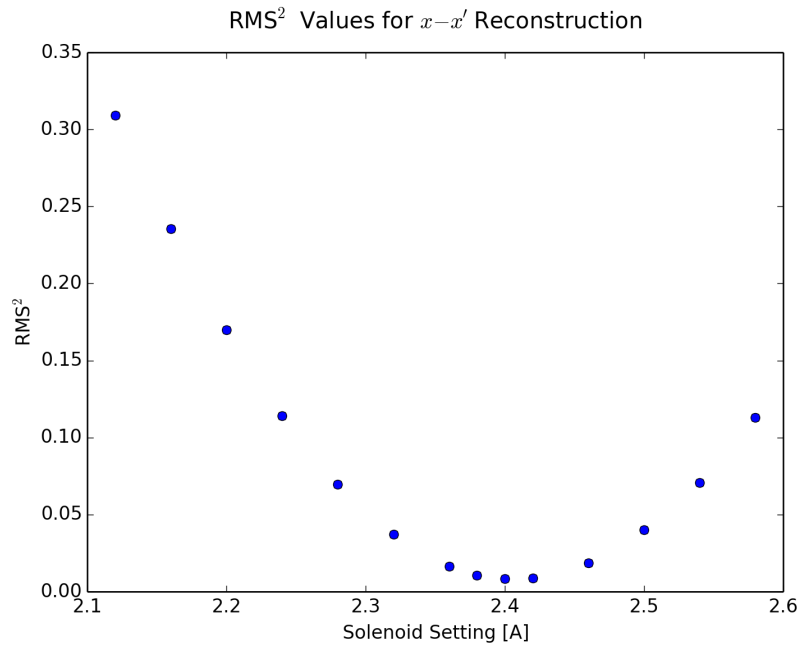


Figure 13: The  $\text{RMS}^2$  values of each of the  $x$  profiles obtained from the view screen data. The plot takes the form of a parabola as expected.

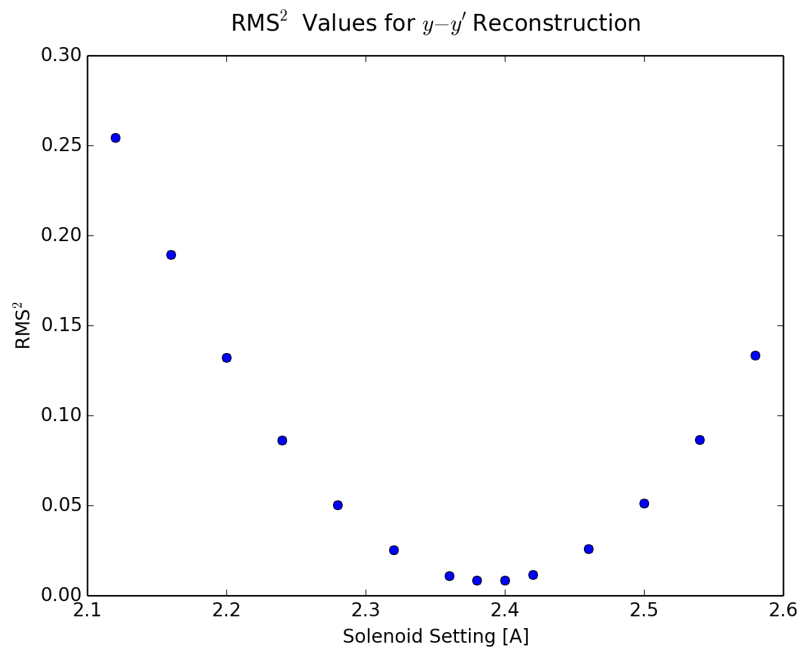


Figure 14: The  $\text{RMS}^2$  values of each of the  $y$  profiles obtained from the view screen data. The plot takes the form of a parabola as expected.

### 3.4 Web Application

The final step to be considered in the implementation of phase space tomography is the development of a simple and intuitive interface to be used by the operators. Previous progress was made by D. Tattan [4] and S. Marcano [6] in developing this interface as a web application using a Python web framework known as Flask [7]. The web application was capable of displaying a set of XML files corresponding to different settings/profiles based on a selected beamline, beampath, profile monitor and date. The user could then select the profiles/scans to use for the tomography reconstruction and adjust the MENT input parameters as required. In the case where the user chose to run tomography, they would be directed to a new interface showing the resulting phase space reconstruction as well as the 1D profiles, profile integrals, RMS<sup>2</sup> plots and MENT output.

An additional interface within this web application has now been developed and is responsible for allowing the user to upload new data for tomography. Once the user specifies a beamline, beampath and profile monitor, the interface guides the user through a list of current/voltages to apply to a ramping element that is referenced from a default XML based on the current configuration. As the user applies each setting, they are asked to upload the corresponding raw datafile obtained from the selected profile monitor and are then shown the corresponding post processed  $x$  and  $y$  profiles as well as the profile integrals and RMS<sup>2</sup> values. Note that the raw datafiles are referenced from the elinac/isac database. If the user recognizes that the scans contain errors such as beam loss, they can abort and redo the scan. Once the scan is complete, all of the uploaded profiles as well as the post processed profiles are saved in XML files under the same Scan ID and can later be used to attempt tomography

reconstructions using the previously developed interface. Figures 15 and 16 each show one half of this interface in an example where the user attempts to take scans in the egun-elbd beampath using the FWS1 profile monitor.

In general, the user will not be expected to select the ramping element and the settings for the ramping element. The optimal settings will be stored in scan XML files that the user can view by selecting View Default XML under More Options. If the user would like to adjust the list of settings or the ramping element, they are allowed to upload their own scan XML file. Ultimately, this interface provides a simple and effective method of enabling users to run phase space tomography.

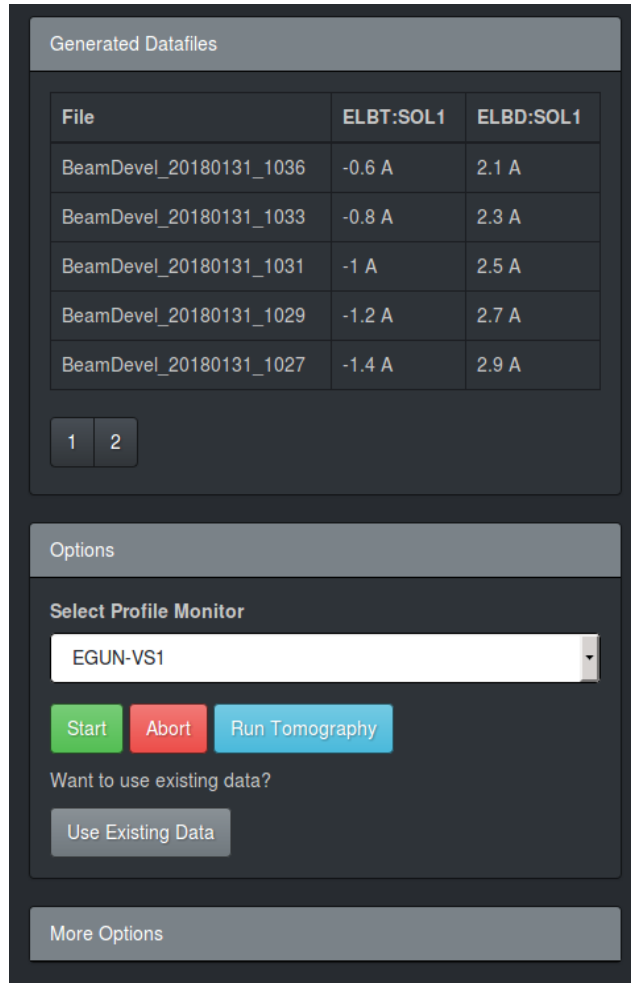


Figure 15: First half of the scan interface for the tomography application. *Generated Datafiles* shows the name of the raw datafiles that have currently been uploaded and their corresponding settings. *Options* allows the user to select a profile monitor and start the scan process. If the user begins to notice issues such as beam loss, the scan can be aborted. Once the scan is complete, the user will be allowed to immediately run tomography. Finally, *More Options* allows the user to view the default XML specifying the ramping elements and settings for the current configuration as well as upload their own XML file if they would like to use a different ramping element or list of settings.

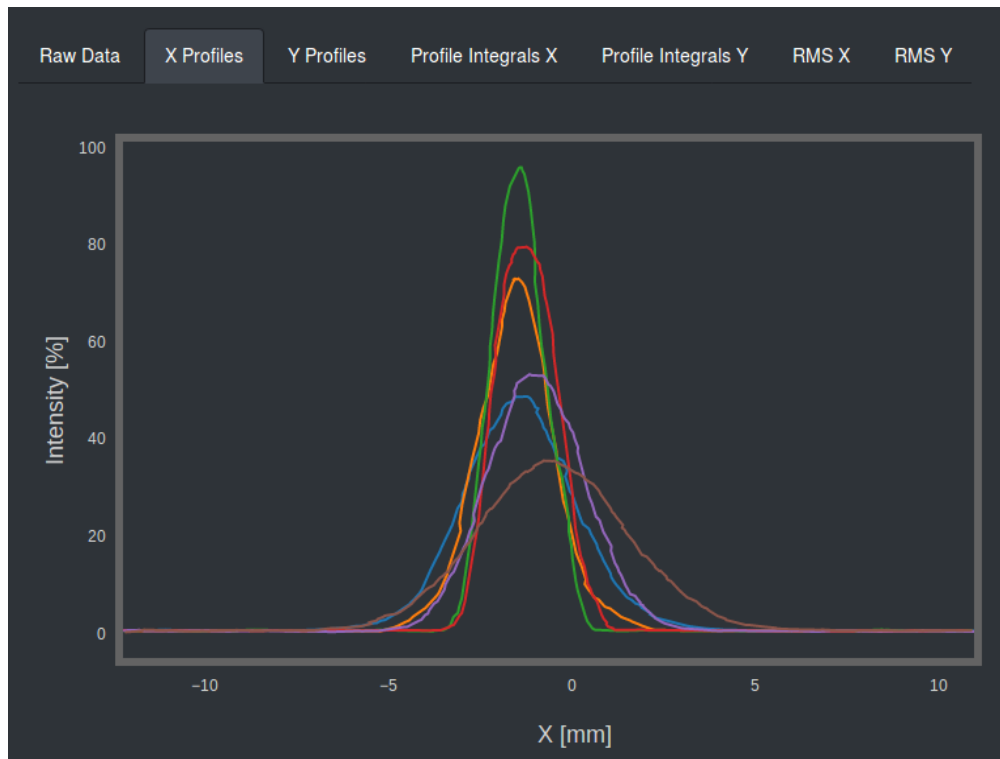


Figure 16: Second half of the scan interface for the tomography application. Similar to the webpage responsible for showing the MENT output, the user can view the post processed  $x$  and  $y$  profiles as well as the integral and RMS plots. The integral and RMS plots can be used to determine if the scan is not running correctly and needs to be aborted.

## 4.0 Conclusions

The phase space reconstructions provided by MENT for the cases involving simulated data proved to be very successful. While this method of generating simulated data using multivariate distributions with additional polynomial shifts provides an effective method for testing and verifying the results of MENT, it can additionally be used to determine sets of optimal settings for specific element configurations and diagnose problems with unsuccessful tomography reconstructions involving real data.

The horizontal and vertical phase space reconstructions that were completed using EGUN:SOL1 as the ramping element and ELBT:VS2 as the view screen for obtaining profiles provided promising results based on comparisons of the RMS and emittance values obtained from MENT with those obtained from TRANSOPTR. The percent difference for the emittance values was 0.037% for both reconstructions. While this result further emphasizes the potential of phase space tomography to serve as a powerful tool for reconstructing phase space, it also emphasizes another technique for obtaining the 1D profiles required by MENT. This technique involves obtaining the profiles from view screen data by applying image processing techniques including filtering and then summing the relevant greyscale pixel values along each row or column. Ultimately, these results emphasize that view screens may prove to be a useful additional tool for measuring profiles and will provide more configurations in which tomography can be tested and applied.

The web application for tomography now includes an additional interface that allows the user to upload new data for tomography. The user is instructed to apply a specific list of settings to a specific ramping element based on the selected beamline, beampath and profile monitor and is then allowed to upload

and view the profiles from their corresponding raw datafiles. In addition to the post processed profiles, the profile integrals and RMS<sup>2</sup> plots are also displayed and will provide additional information in regards to determining if the scan needs to be aborted. Overall, this application will serve as a major step to ensuring that tomography is simple and easy to use and emphasizes another advantage of applying the MENT algorithm.

## 5.0 Recommendations

Overall, the phase space reconstructions shown in this report and previous reports emphasize that phase space tomography using MENT may prove to be an invaluable tool in completing phase space reconstructions. Recommended future steps would be to continue testing phase space tomography on different locations along the isac and elinac beamlines using different ramping element and profile monitor configurations. This will be useful for providing additional validation in regards to the overall effectiveness of phase space tomography and will also be useful for providing further testing for the web application.

In regards to the web application, additional updates will be required once a system for setting and getting PV values is successfully established. Currently, the application relies on the user to set each setting on the specified ramping element and upload each corresponding raw datafile from the selected profile monitor. However, once the set/get system is established, it will be very useful to modify the application such that it sets each of the PV values and gets each of the corresponding profiles as this will prevent the user from having to complete any additional tasks after starting the scan. It should be noted that this will require the use of websockets if the interface is to be automatically updated after each profile is obtained.

## A Phase Space

This appendix focuses on providing a simple and intuitive explanation of the motivation behind phase space. To begin with, it is important to note that it is very common in accelerator physics to use local Cartesian coordinates with  $s$  as the independent variable. This type of coordinate system is known as the **Frenet Serret** coordinate system and is shown in Figure 17. Since  $s$  serves as the independent variable in this system, primes refer to differentiation with respect to  $s$  such that  $x' = dx/ds$  and  $y' = dy/ds$ .

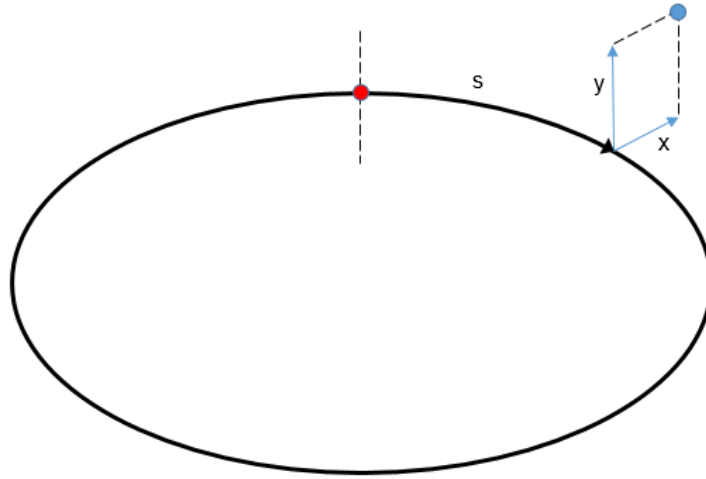


Figure 17: Visual representation of the Frenet Serret coordinate system. The red point represents the reference point at which  $s = 0$  and the black line represents the design orbit.

The equation of motion of a single beam particle or a charged particle under the influence of an external field assuming there is no momentum spread  $\Delta p$  is given by the equation  $x'' + \kappa(s)x = 0$  where  $\kappa(s)$  is the **focusing function** and depends on the external field. This equation is known as **Hill's equation**. The general solution to Hill's equation is

$$x(s) = Cw(s) \cos(\psi(s) + \phi) \quad (2)$$

where  $w(s)$  and  $\psi(s)$  are the amplitude and phase functions respectively. Substitution of this equation back into Hill's equation along with several clever rearrangements gives

$$\gamma x^2 + 2\alpha x x' + \beta x'^2 = C^2 \quad (3)$$

where  $\alpha = -ww'$ ,  $\beta = w^2$  and  $\gamma = \frac{1}{w^2} + w'^2$  are referred to as the **Courant Snyder** or **Twiss** parameters and  $C$  is referred to as the **Courant Snyder invariant** or the **single particle emittance**. Equation 2 represents a tilted ellipse in **phase space** and is graphed in Figure 18.

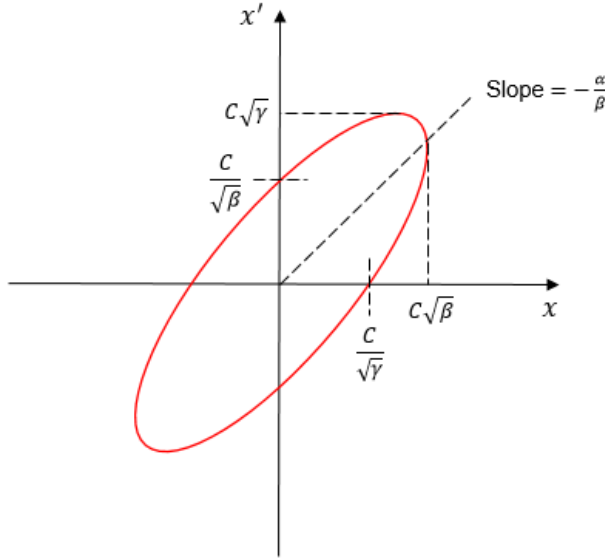


Figure 18: Graph of the phase space ellipse corresponding to Equation 2.

In accelerator physics, it is necessary to consider a particle ensemble as opposed to a single particle. If we assume that a given particle ensemble is only acted upon by conservative forces and thus satisfies Hamilton's equations of motion, then it can be shown by **Liouville's theorem** that the volume occupied by a number of particles is invariant. In the case where the motion of the particles along the three unit basis vectors in 6D phase space is uncoupled and we can thus consider the projections of this phase space onto any plane such as the  $x - x'$  plane, we can establish that all particles within a 2D

phase space ellipse will remain in that ellipse as the beam travels through the beamline. Mathematically, this can be stated as  $\iint dx dx' = \text{Constant}$ . In the case of a particle ensemble, we can simply choose the particle whose ellipse has the maximum amplitude  $C$ . We then know that all particles within this ellipse will stay within this ellipse and can thus predict the positions and motion of the beam without having to calculate the trajectory of each individual particle. Since the equation of this ellipse corresponds to Equation 2, we know that the area enclosed by the ellipse is given by  $\pi C^2$  since  $\beta\gamma - \alpha^2 = 1$ . This leads to the definition of **beam emittance** which is essentially a measure of the size of the beam. Beam emittance is defined to be proportional to the area of this phase space ellipse and is given by

$$\varepsilon \equiv \frac{\pi C^2}{\pi} = C^2 \tag{4}$$

The concept of phase space and beam emittance is a powerful tool in accelerator physics for describing beams. The phase space ellipse at any other point along the beamline can be determined simply by applying the corresponding linear transformations as shown below.

$$\begin{pmatrix} x(s) \\ x'(s) \end{pmatrix} = \begin{pmatrix} C(s) & S(s) \\ C'(s) & S'(s) \end{pmatrix} \begin{pmatrix} x_0(s) \\ x'_0(s) \end{pmatrix} \tag{5}$$

where  $C(s)$  and  $S(s)$  are cosine and sine like functions respectively. This ultimately helps to emphasize the importance of developing a simple and effective algorithm for reconstructing phase space distributions.

## B Lattice Elements

In accelerator physics, the **design orbit** refers to the ideal orbit on which the particles should move. When a beam travels through a beamline, there are usually several instances where we will need to bend and focus the beam in order to ensure that the beam follows its design orbit as closely as possible. This is done using electromagnetic forces imposed by **lattice elements**. The two most common lattice elements are **dipoles** and **quadrupoles** which are responsible for steering and focusing the beam respectively. The potential field of these elements as well as any other higher order multipole can be described mathematically using the Fourier Series:

$$\phi = \sum_{m=0}^{\infty} r^m (A_m \cos(m\theta) + B_m \sin(m\theta)) \quad (6)$$

where  $r$  and  $\theta$  are polar coordinates on the field of the plane. This is called a **multipole field expansion** and it allows us to compute different orders/effects of the field as opposed to the total field. Of course the field can be determined simply by computing the gradient of  $\phi$ . For  $m = 0$  we have  $\phi = A_0$  and thus  $\vec{B} = \vec{0}$ . For  $m = 1$  we have

$$\phi = A_1 r \cos \theta + B_1 r \sin \theta = A_1 x + B_1 y \quad (7)$$

and thus  $\mathbf{B} = (-A_1, -B_1)$ . This term is referred to as the **dipole term** or **dipole field**. It represents the constant field produced by a configuration consisting of two magnets or electrodes and is responsible for bending the beam. For  $m = 2$  we have

$$\phi = A_2 r^2 \cos 2\theta + B_2 r^2 \sin 2\theta = A_2(x^2 - y^2) + B_2 2xy \quad (8)$$

and thus  $\mathbf{B} = -2(A_2x + B_2y, B_2x - A_2y)$ . This term is referred to as the **quadrupole term** or quadrupole field. It is a linear field that results from a configuration consisting of four magnets or electrodes and is responsible for focusing the beam in one direction and defocusing the beam in the other. Higher order fields are normally used to correct higher order aberrations in beams. For example, a sextupole aberration would be corrected by applying a sextupole magnet with opposing polarity so as to cancel the aberration. Note that a sextupole corresponds to  $m = 3$  and consists of 6 magnets/electrodes. In general, the number of magnets/electrodes corresponding to a given order will be equal to  $2m$ . Figure 19 shows the fields and magnet/electrode configurations corresponding to the first three orders.

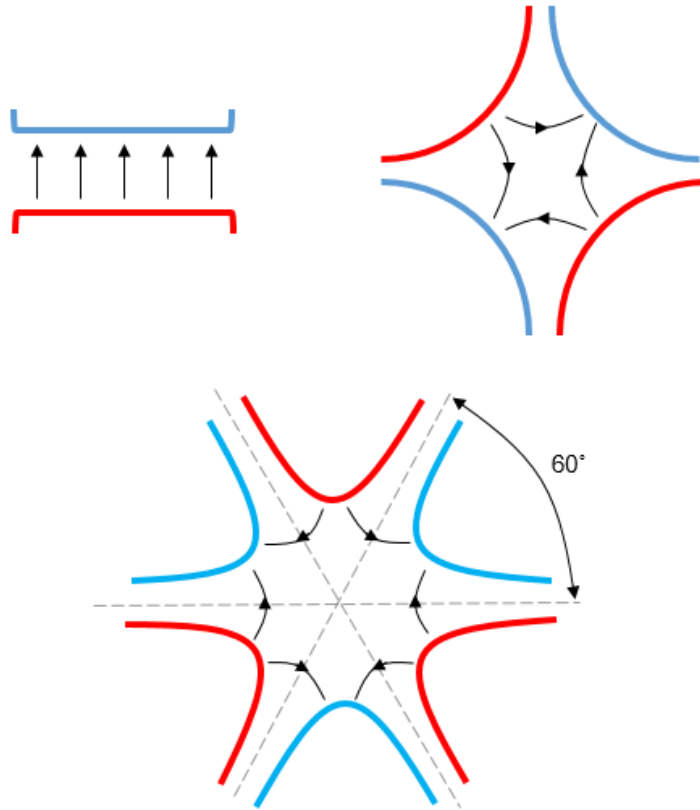


Figure 19: Multipoles corresponding to the first three orders. Top left is a dipole, top right is a quadrupole and bottom is a sextupole. Red and blue correspond to North and South respectively. Black lines indicate magnetic field lines.

## References

- [1] G. Minerbo, “Ment: A maximum entropy algorithm for reconstructing a source from projection data,” vol. 10, pp. 48–68, 05 1979.
- [2] J. J. Scheins, “Tomographic reconstruction of transverse and longitudinal phase space distributions using the maximum entropy algorithm.”
- [3] R. Baartman, “`transoptr` changes since 1984,” no. TRI-BN-16-06, 2016.
- [4] D. Tattan, “On the Beam Tomography Web Application,” Tech. Rep. TRI-BN-17-09, TRIUMF, 2017.
- [5] S. van der Walt, J. L. Schönberger, J. Nunez-Iglesias, F. Boulogne, J. D. Warner, N. Yager, E. Gouillart, T. Yu, and the scikit-image contributors, “scikit-image: image processing in Python,” *PeerJ*, vol. 2, p. e453, 6 2014.
- [6] S. Marcano, “Customizing Web Applications for Beam Tomography,” Tech. Rep. TRI-BN-17-01, TRIUMF, 2017.
- [7] *Flask Documentation*. <http://flask.pocoo.org/docs/0.12/>.